



Stars that Move Together Were Born Together

Harshil Kamdar¹, Charlie Conroy¹, Yuan-Sen Ting^{2,3,4,7}, Ana Bonaca¹, Martin C. Smith⁵, and Anthony G. A. Brown⁶

¹Harvard-Smithsonian Center for Astrophysics, Cambridge, MA 02138, USA

²Institute for Advanced Study, Princeton, NJ 08540, USA

³Department of Astrophysical Sciences, Princeton University, Princeton, NJ 08544, USA

⁴Observatories of the Carnegie Institution of Washington, 813 Santa Barbara Street, Pasadena, CA 91101, USA

⁵Key Laboratory for Research in Galaxies and Cosmology, Shanghai Astronomical Observatory, Chinese Academy of Sciences, 80 Nandan Road, Shanghai 200030, People's Republic of China

⁶Leiden Observatory, Leiden University, P.O. Box 9513, 2300RA Leiden, The Netherlands

Received 2019 April 3; revised 2019 September 10; accepted 2019 October 1; published 2019 October 15

Abstract

It is challenging to reliably identify stars that were born together outside of actively star-forming regions and bound stellar systems. However, conatal stars should be present throughout the Galaxy, and their demographics can shed light on the clustered nature of star formation and the dynamical state of the disk. In previous work we presented a set of simulations of the Galactic disk that followed the clustered formation and dynamical evolution of 4 billion individual stars over the last 5 Gyr. The simulations predict that a high fraction of comoving stars with physical and 3D velocity separation of $\Delta r < 20$ pc and $\Delta v < 1.5$ km s⁻¹ are conatal. In this Letter, we use *Gaia* DR2 and LAMOST DR4 data to identify and study comoving pairs. We find that the distribution of relative velocities and separations of pairs in the data is in good agreement with the predictions from the simulation. We identify 111 comoving pairs in the solar neighborhood with reliable astrometric and spectroscopic measurements. These pairs show a strong preference for having similar metallicities when compared to random field pairs. We therefore conclude that these pairs were very likely born together. The simulations predict that conatal pairs are born in clusters that follow the overall cluster mass function and in relatively young (<1 Gyr) star clusters. *Gaia* will eventually deliver well-determined metallicities for the brightest stars, enabling the identification of thousands of conatal pairs due to disrupting star clusters in the solar neighborhood.

Key words: Galaxy: evolution – Galaxy: kinematics and dynamics – open clusters and associations: general

1. Introduction

Close stars moving together in the Galaxy may hold valuable clues related to star formation (e.g., Parker et al. 2011; Reipurth & Mikkola 2012) and the dynamical history of the Galaxy (e.g., Weinberg et al. 1987; Monroy-Rodríguez & Allen 2014). Pairs of stars that are close together ($\lesssim 1$ pc) are likely gravitationally bound (Jiang & Tremaine 2010). Pairs further apart ($\gtrsim 1$ pc) are less likely to be gravitationally bound and may be associated with dissolving clusters (Kouwenhoven et al. 2010), thereby allowing us to study cluster disruption and the star formation history of the Milky Way (e.g., Bland-Hawthorn et al. 2010).

The study of comoving pairs using proper motions has a rich history (e.g., Poveda et al. 1994; Chanamé & Gould 2004; Shaya & Olling 2010; Tokovinin & Lépine 2012; Alonso-Floriano et al. 2015). Recent work (e.g., Andrews et al. 2017a, 2017b, 2019; Oelkers et al. 2017; Oh et al. 2017; Price-Whelan et al. 2017; Bochanski et al. 2018; El-Badry & Rix 2018, 2019; Simpson et al. 2018; Jiménez-Esteban et al. 2019) has shown the power of using *Gaia* to study comoving pairs. The availability of 6D phase-space information for millions of stars from *Gaia* DR2 and complementary data from ground-based spectroscopic surveys provide a unique opportunity to understand the nature of comoving pairs. However, ab initio simulations of galaxy formation currently do not offer the resolution necessary to interpret the small-scale phase-space structure observed in *Gaia* data.

In Kamdar et al. (2019, hereafter K19) we presented simulations that resolve the dynamical evolution of individual stars comprising the disk over the past 5 Gyr. A key prediction of the fiducial simulation presented in K19 is the high fraction of pairs at large separations (up to 20 pc) and at low relative velocities (up to 1.5 km s⁻¹) that were born together (conatal). In this Letter we use *Gaia* DR2 and the Large Sky Area Multi-Object Fibre Spectroscopic Telescope (LAMOST) DR4 to test the predictions presented in K19 and explore the nature of comoving pairs.

2. Simulations and Data

In K19 we introduced a new set of simulations that were the first of their kind to model the full population of stars (younger than 5 Gyr) that comprise a Milky Way-like disk galaxy. All stars are born in clusters with a range of initial conditions informed by observations and detailed simulations. The dynamical evolution of 4 billion stars was performed with orbit integration of test particles coupled to a realistic time-varying galactic potential, which includes a disk, halo, bulge, bar, spiral arms, and giant molecular clouds (as perturbers). In K19, we compare the age-velocity dispersion, the surface density profile, and the solar neighborhood metallicity distribution function of the fiducial simulation to the data and find encouraging agreement. These simulations predict a rich structure in the combined phase and chemical space that should inform our understanding of the nature of clustered star formation.

The fiducial simulation presented in K19 has both nonaxisymmetries in the potential (bar, spiral arms, and giant

⁷ Hubble Fellow.

molecular clouds) and clustered star formation. We also ran two control simulations: (1) a simulation with a static axisymmetric potential and with clustered star formation, and (2) a simulation with nonaxisymmetric perturbations (with bar and spiral arms) but with no clustered star formation (hereafter referred to as the NCSF simulation). The three different simulations allow us to study the scales at which structure due to clustered star formation and structure due to resonances by the nonaxisymmetries in the Milky Way will manifest itself on the combined chemodynamical space.

To enable a fair comparison to *Gaia* and spectroscopic surveys, we create mock catalogs of *Gaia* DR2–like solar neighborhoods. The solar neighborhood sphere is centered at $(-8.2, 0.0, 0.027)$ kpc (Chen et al. 2001; Bland-Hawthorn & Gerhard 2016) and has a radius of 1 kpc. We use the MIST stellar evolutionary tracks (Choi et al. 2016) and the C3K stellar library (C. Conroy et al. 2019, in preparation) to derive photometry for the simulated stars using a Kroupa initial mass function (Kroupa 2001). *Gaia* DR2 contains the radial velocities for about 7 million stars with $G_{\text{RVs}}^{\text{ext}}$ —to mimic this selection, we calculate $G_{\text{RVs}}^{\text{ext}}$ using the Tycho color transformations presented in Sartoretti et al. (2018) and apply the same cut.

An accurate error model is essential for comparisons between simulations and observations. The error in the parallax is approximated by a simple error floor of 0.04 mas (Lindgren et al. 2018). The dependence of proper motion and radial velocity errors is a complex function of several parameters; we fit a Gaussian mixture model with 20 components to the combined $(G, G_{\text{BP}} - G_{\text{RP}}, \sigma_{\mu_{\alpha^*}}, \sigma_{\mu_{\delta}})$ and $(G, G_{\text{BP}} - G_{\text{RP}}, \sigma_{\text{RV}})$ spaces, respectively, and sample from the conditional distributions for the respective errors given G and $G_{\text{BP}} - G_{\text{RP}}$.

We start with the 6D *Gaia* DR2 (*Gaia* Collaboration et al. 2018) catalog from Marchetti et al. (2019). We cross-matched with LAMOST DR4 catalog (with duplicates removed) for the same 1 kpc sphere around the solar position as in the simulations. The search radius for the cross-match is limited to $3''$. LAMOST DR4 (Deng et al. 2012) provides T_{eff} , $[\text{Fe}/\text{H}]$, radial velocities, and $\log g$ using LAMOST’s spectroscopic pipeline (Wu et al. 2011; Luo et al. 2015). Only stars that have radial velocity measurements in *Gaia* DR2 are considered for the work presented here since LAMOST RVs have errors between 5 and 7 km s⁻¹.

We impose the following selection criteria on the *Gaia* data considered in this analysis: (1) number of visibility periods ≥ 8 , (2) number of RV transits ≥ 3 , (3) renormalized unit weight error (RUWE) ≤ 1.6 (the results presented in this work do not change when making the more conservative ≤ 1.4 cut used in Lindgren 2018),⁸ and (4) bad RVs found in Boubert et al. (2019) have been removed. We also require signal-to-noise ratio $(\text{S}/\text{N})_i > 40$ in the LAMOST data to ensure small measurement uncertainties. After making these quality cuts, the quoted mean and median uncertainties on the radial velocity are 2.15 and 1.32 km s⁻¹ and on $[\text{Fe}/\text{H}]$ are 0.037 and 0.024 dex, respectively. We emphasize that it is the relative difference between metallicities that is important for this work, rather than the absolute metallicity scale. We have also identified a

significant correlation between the metallicity difference and T_{eff} difference for pairs of stars, which we interpret as a systematic uncertainty on the derived metallicities. To limit this systematic uncertainty, we restrict our analysis to pairs with a temperature difference of $\Delta T_{\text{eff}} < 200$ K.

The overall selection function for *Gaia* is not critical for this work because we only consider fractional quantities when comparing between data and simulations. We have also explored the impact of the LAMOST selection function on the population of pairs. We find, for example, no statistically significant difference in the distribution of physical separations for pairs with and without LAMOST data, leading us to conclude that the LAMOST selection function does not result in a biased population of pairs.

Since the simulations in K19 do not include binarity, it is important to discuss how to isolate the phase-space signature of disrupting star clusters and avoid contamination from wide binaries in the data. For our analysis, we will only consider pairs with separations greater than 2 pc, since the Jacobi radius is ≈ 2 pc for $\sim 1M_{\odot}$ stars in the solar neighborhood (Yoo et al. 2004; Jiang & Tremaine 2010). In addition, Jiang & Tremaine (2010) predict a trough in the distribution of wide binaries between ~ 1 and 10 times the Jacobi radii, which corresponds to separations between ~ 2 and 18 pc in the solar neighborhood. Consequently, we expect the contamination from wide binaries for the spatial scales being considered in this work to be low.

Moreover, comoving pairs could be a part of known bound clusters, moving groups or OB associations in the Milky Way. We choose to exclude pairs from these to isolate the signal of star clusters that are disrupting. The exploration of the phase-space signature in data and simulations for bound objects is left for future work. Similar to Oh et al. (2017), we form an undirected graph where stars are nodes, and edges between the nodes exist for comoving pairs of stars. Consequently, a star could have multiple comoving neighbors, and a pair of stars could be directly or indirectly connected via a sequence of edges. The graph is then split into connected components—a connected component is a subgraph of the original graph in which any two nodes are connected to each other by a path—to pick out only mutually exclusive pairs. This additional selection criteria efficiently filters out known open clusters, OB associations, and moving groups.

3. Comoving Pairs in Simulations and Data

In this section we investigate comoving pairs in the simulations and the data. We begin with a pairwise comparison of the fraction of pairs as a function of separation and velocity difference in the simulations and in the data in Figure 1. The left panel of Figure 1 shows the fraction of comoving pairs as a function of Δr for the different simulations (dashed lines of different colors) and the data (black solid line) after imposing a $\Delta v < 1.5$ km s⁻¹ cut. At smaller separations, clustering seems to be stronger in the data than in the simulations. The discrepancy at the smallest separations could be due to contamination from wide binaries or hint at complexities in the data regarding star formation that are not adequately modeled in the fiducial simulation.

The right panel of Figure 1 shows the fraction of comoving pairs as a function of Δv for the different simulations and the data with the cut $2 < \Delta r < 20$ pc. The axisymmetric simulation has a notably higher fraction of pairs at lower Δv due to the absence of any large-scale scattering. The NCSF

⁸ The traditional square root of the reduced chi-squared (unit weight error) has a strong dependence on color and magnitude. These dependencies are removed using a renormalization process (Lindgren 2018). The RUWE error provides a more robust indicator of the goodness of fit for the astrometry.

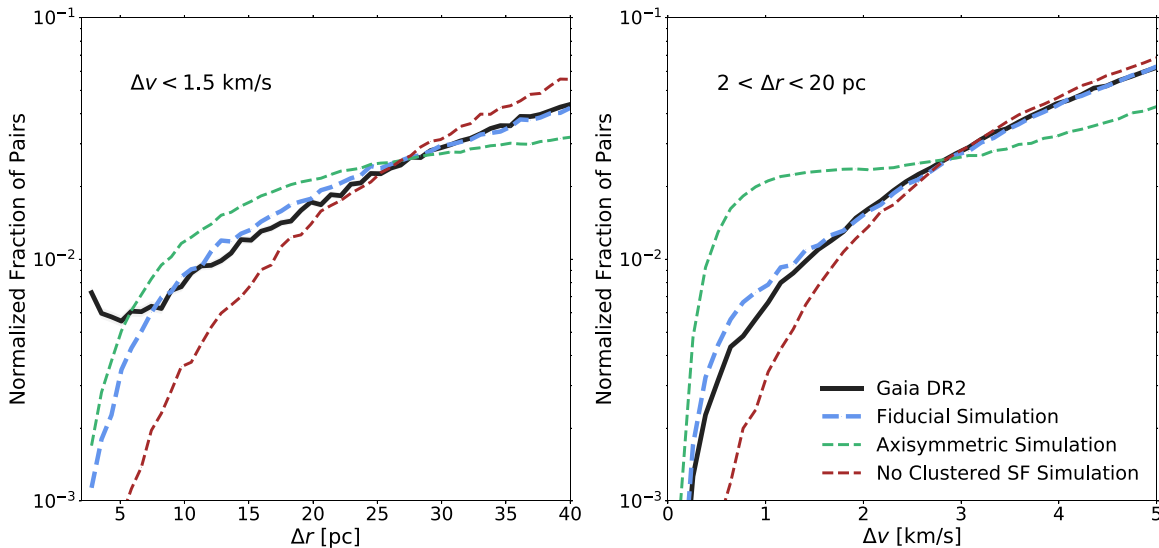


Figure 1. Normalized fraction of pairs as a function of the separation (left panel) and velocity difference (right panel)—data are the black line, Poisson errors for the data are in gray (too small to be seen), fiducial simulation is the dashed blue line, axisymmetric simulation is the dashed green line, and NCSF is the dashed red line. All three simulations underestimate clustering at the smallest separations ($\Delta r < 5$ pc). The disagreement may arise from contamination from disrupting wide binaries, or due to lack of complexity in our prescription for star formation. The differences in the fraction of pairs for the velocity difference in the simulations and the data indicate that the count of pairs at small velocities is sensitive to both clustered star formation and the nonaxisymmetries in the potential of the Milky Way. The fiducial simulation, which has both, agrees better with the data than the other models.

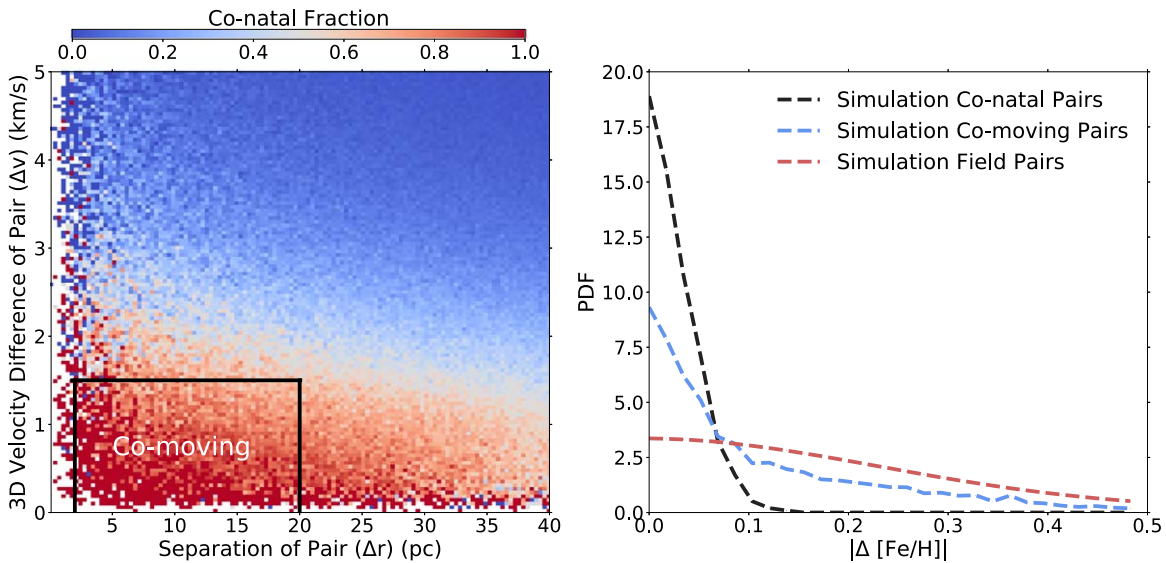


Figure 2. Left panel: conatal fraction of pairs as a function of separation (Δr) and 3D velocity difference (Δv) in the fiducial simulation. Pairs with $2 < \Delta r < 20$ pc and $\Delta v < 1.5$ km s^{-1} have a notably high conatal fraction—the selection box is used to define “comoving” pairs. Right panel: expected difference in metallicities of stars in a pair. The blue line shows the metallicity difference distribution for all comoving pairs, while the red line shows the metallicity difference distribution for random field pairs in the solar neighborhood sample. The black line shows the metallicity difference for the subset of comoving pairs that are also conatal. The simulation adopts $\sigma_{[\text{Fe}/\text{H}]} = 0.03$ dex.

simulation has a notably lower relative fraction at lower Δv due to the absence of clustered star formation. The fiducial simulation, which has both clustered star formation and nonaxisymmetries in the potential, is in excellent agreement with the data.

Figure 2 shows the conatal fraction of comoving pairs in the fiducial simulation presented in K19. The simulation predicts that pairs of stars with a velocity difference up to 1.5 km s^{-1} but a high separation of up to 20 pc are highly likely to be born together. The large physical separation suggests that the comoving pairs of stars are likely part of a disrupting star cluster—studying such conatal pairs in data will provide key insights into star formation in the disk. Consequently, using the

simulation as a prior of sorts, we will use the selection box $2 < \Delta r < 20$ pc and $\Delta v < 1.5$ km s^{-1} to both avoid most wide binaries and look for signatures of dissolving star clusters in the data.

While, as we can see in the left panel of Figure 2, the selection box contains a large number of comoving pairs that are conatal, there is still some contamination (about $\sim 20\%$) from field pairs. To test whether we find a similarly high conatal fraction in data, we can use metallicities since stars born in the same cluster are believed to have essentially identical metallicities (e.g., De Silva et al. 2007; Bovy 2016), modulo atomic diffusion (Dotter et al. 2017), or star–planet interactions (Oh et al. 2018). The right panel of Figure 2 shows

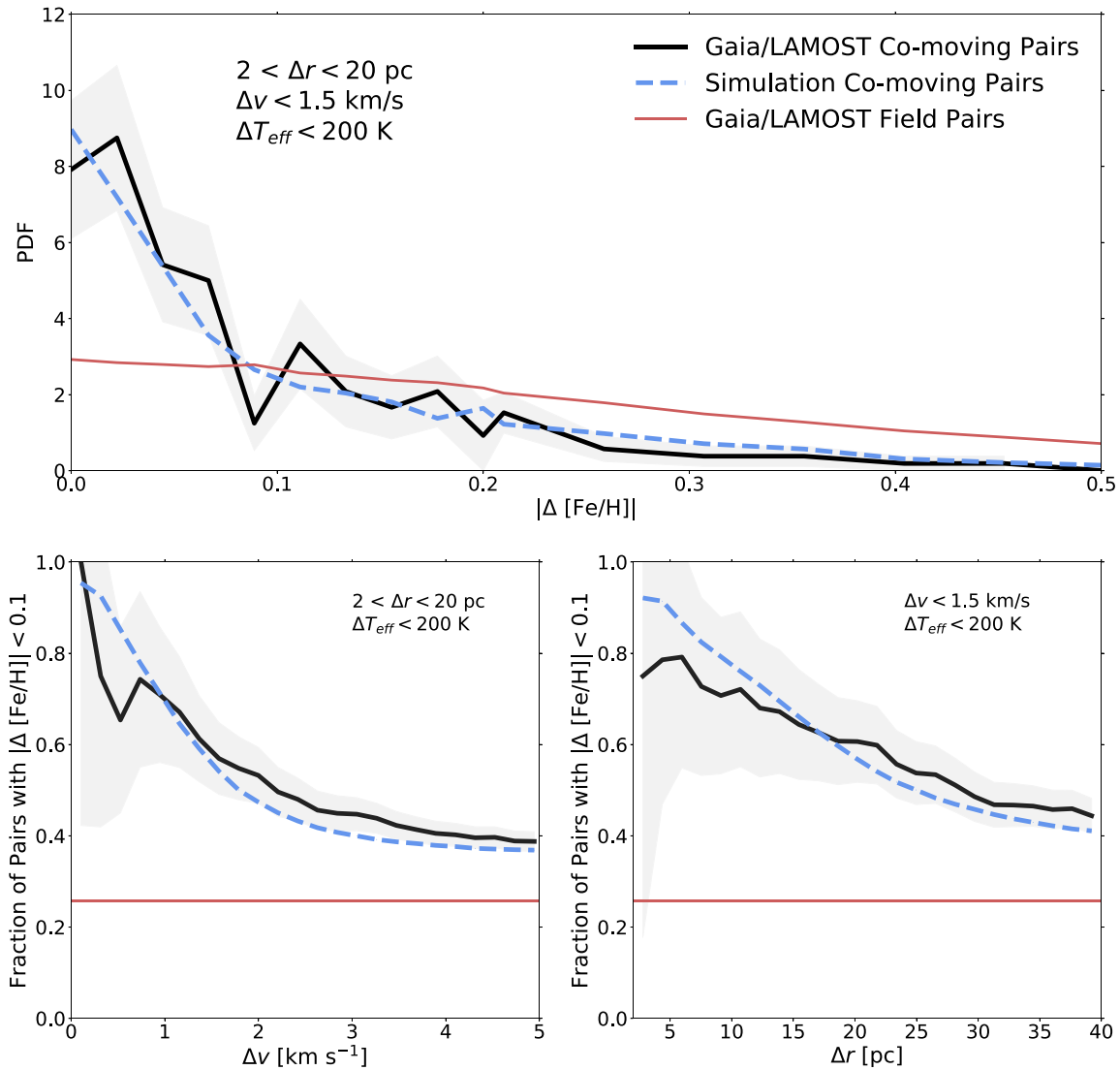


Figure 3. Top panel: $|\Delta[\text{Fe}/\text{H}]|$ distribution for *Gaia*/LAMOST pairs with the selection cuts: $2 < \Delta r < 20$ pc and $\Delta v < 1.5$ km s⁻¹ (black line; with Poisson errors in gray), the simulation with the same Δr and Δv cuts (dashed blue line), and random field *Gaia*/LAMOST pairs (red line). The metallicity difference distribution for the simulation (with $\sigma_{[\text{Fe}/\text{H}]} = 0.03$ dex) and the data agree remarkably well. Bottom left panel: the fraction of pairs with $|\Delta[\text{Fe}/\text{H}]| < 0.1$ dex for data (black line; Poisson errors in gray) and the fiducial simulation (blue dashed line) as a function of different velocity difference cuts after already imposing $\Delta r < 20$ pc. Both the simulation and the data show a similar peak of low-metallicity difference pairs at low-velocity differences. As Δv increases, the fraction of pairs with $|\Delta[\text{Fe}/\text{H}]| < 0.1$ approaches the value for random field pairs (red line). Bottom right panel: the fraction of pairs with $|\Delta[\text{Fe}/\text{H}]| < 0.1$ dex for data (black line; Poisson errors in gray) and the fiducial simulation (blue dashed line) as a function of different separation cuts after already imposing $\Delta v < 1.5$ km s⁻¹. Both the simulation and the data show a similar peak of low-metallicity difference pairs at low separations. As Δr increases, the fraction of pairs with $|\Delta[\text{Fe}/\text{H}]| < 0.1$ approaches the value for random field pairs (red line).

expectations for the metallicity ($[\text{Fe}/\text{H}]$) difference distribution of comoving pairs. The black line shows pairs of stars known to be conatal in the selection box, the blue line shows all pairs of stars in the selection box, and the red line shows random field pairs. The measurement uncertainty in $[\text{Fe}/\text{H}]$ in the simulations is 0.03 dex. The selection criteria are effective at picking out conatal pairs, but there is still enough contamination from field pairs for there to be a tail at larger metallicity differences. The blue line will be used to compare to the *Gaia*/LAMOST cross-match.

The top panel of Figure 3 shows the metallicity difference ($|\Delta[\text{Fe}/\text{H}]|$) for comoving pairs with $2 < \Delta r < 20$ pc and $\Delta v < 1.5$ km s⁻¹. The agreement between the data and the simulation (which has a fiducial $\sigma_{[\text{Fe}/\text{H}]} = 0.03$ dex as a mock observational uncertainty) is very good. Moreover, the distribution of metallicity differences is significantly narrower

than the field metallicity difference distribution, suggesting that the comoving pairs we have identified are conatal.

The bottom left panel of Figure 3 shows the fraction of pairs with $|\Delta[\text{Fe}/\text{H}]| < 0.1$ as a function of different velocity cuts after already imposing $2 < \Delta r < 20$ pc. The fraction of stars with a low-metallicity difference quickly drops for velocity differences larger than ~ 1 – 1.5 km s⁻¹ in both the data and the simulation. The fraction of pairs with low-metallicity differences approaches that of the field pairs’ at progressively larger Δv cuts.

The bottom right panel of Figure 3 shows the fraction of pairs with $|\Delta[\text{Fe}/\text{H}]| < 0.1$ as a function of different separation cuts after already imposing $\Delta v < 1.5$ km s⁻¹. The fraction of stars with a low-metallicity difference drops relatively smoothly as a function of separation for both the simulation and the data—this trend is also clearly visible in Figure 2. The fraction of pairs with low-metallicity differences approaches

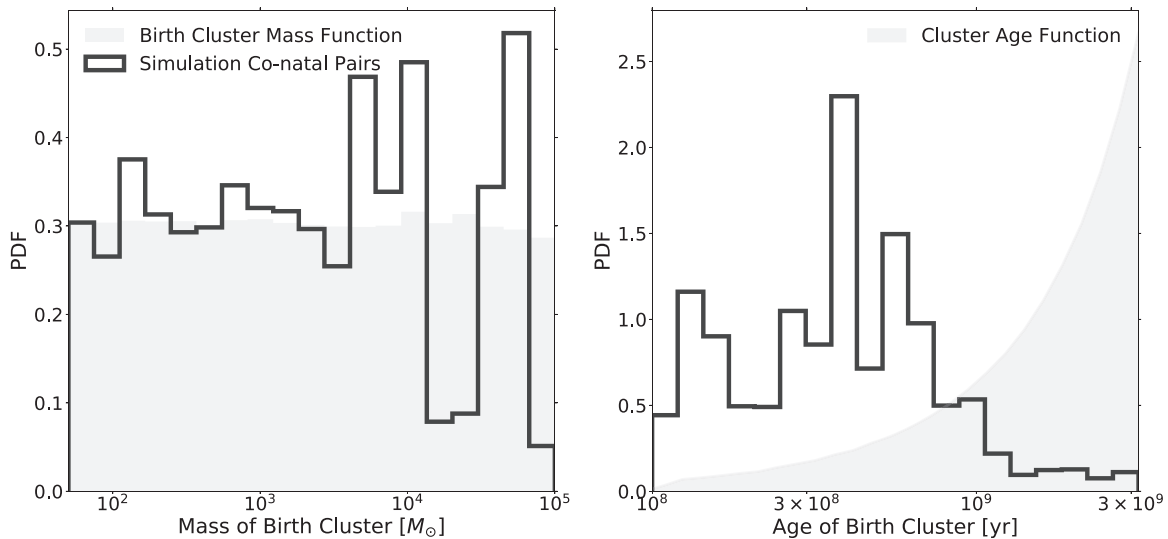


Figure 4. Demographics of simulated comoving pairs that are conatal. Left panel: the distribution of the masses of the birth clusters of the conatal pairs in the simulation (black) compared to the overall birth cluster mass function (gray). Right panel: the distribution of ages of the conatal pairs in simulation (black) compared to the overall cluster age function (gray).

Table 1
Catalog of Comoving Pairs Analyzed in This Work

Star 1 <i>Gaia</i> DR2 ID	Star 2 <i>Gaia</i> DR2 ID	Δr (pc)	Δv (km s $^{-1}$)	$ \Delta[\text{Fe}/\text{H}] $ (dex)
454335594920988288	454131631217853312	19.518	0.363	0.041
2130506398193844352	2128941861868381952	18.991	1.347	0.043
1897440689367972096	1897440689367972736	4.447	1.427	0.060
946471222781159040	946435007617437056	6.852	0.978	0.630
893835131555196928	881823826013408384	7.434	0.901	0.059
3992114209767880960	3994508877374172160	17.760	1.249	0.007

Note. The catalog is available in its entirety for download at <http://harshilkamdar.github.io/2019/04/03/pairs.html>.

that of the field pairs’ at progressively larger Δr cuts. Taken together, the results in Figure 3 indicate that the final selection cuts of $2 < \Delta r < 20$ pc and $\Delta v < 1.5$ km s $^{-1}$ lead to a fairly clean sample ($\sim 80\%$ pure) of comoving pairs that were born together.

The simulation offers the opportunity to identify properties of the birth sites of the conatal pairs. The left panel of Figure 4 shows the mass of the birth cluster for the conatal comoving pairs in the selection box in Figure 2 compared to the overall birth cluster mass function (BCMF; the mass of the birth cluster of a random subsample of stars). The clusters that give birth to comoving pairs are a fair tracer of the underlying BCMF. The right panel of Figure 4 shows the age of the birth cluster for the conatal comoving pairs in the selection box shown in Figure 2 compared to the overall cluster age function. The clusters that give birth to conatal comoving pairs are mostly younger than 1 Gyr.

The age distribution of these clusters offers a noteworthy parallel to the discussion of visibility timescale presented in K19, where we argued that the phase-space signature of stars born in clusters should be visible up to 1 Gyr. We can test the predictions made above in the future by analyzing the distribution of comoving pairs in color–magnitude diagram space, where we should be able to tell the difference between 100 Myr stars and 1 Gyr stars (for the more massive stars).

4. Summary

In this Letter we have presented evidence that comoving pairs of stars (identified as having relative physical separation $2 < \Delta r < 20$ pc, and relative velocity $\Delta v < 1.5$ km s $^{-1}$) were very likely born together. Moreover, we have shown that the distribution of pairwise velocities and physical separation is sensitive to both clustered star formation and nonaxisymmetries of the Galactic potential. The simulation presented in K19 is able to reproduce both of these distributions. Furthermore, the simulation predicts that the conatal comoving pairs were born in preferentially high-mass and relatively young clusters relative to the field population. Table 1 lists all 111 pairs in our final catalog and their properties.

The primary metric used here for determining whether a pair is conatal is the metallicity difference ($|\Delta[\text{Fe}/\text{H}]|$). For this we used data from the low-resolution LAMOST spectroscopic survey since it contains far more stars in the solar neighborhood than other surveys such as APOGEE, RAVE, GALAH, etc. Follow-up high-resolution spectra of these comoving pairs are required to confirm the chemical similarity of the pairs, which in turn would bolster the argument that the pairs share a common birth site. *Gaia* DR4 will deliver S/N ~ 50 spectra for stars with $G \sim 12$, allowing calculations of $[\text{Fe}/\text{H}]$ with uncertainties ≤ 0.05 dex (Recio-Blanco et al. 2016; Ting et al. 2017). The simulations predict that we could study thousands of comoving pairs due to disrupting star clusters in the solar neighborhood using *Gaia* alone. This will be complemented

well by data from upcoming surveys such as SDSS–V and 4MOST.

Comoving pairs offer novel constraints on the nature of clustered star formation and the recent dynamical history of the disk. However, pairs offer a limited ($N = 2$) view of the phase-space structure of stars in the disk. Additional insight will be gained by considering the general clustering properties of stars in various phase-space projections. This will be the subject of future work.

We thank Adrian Price-Whelan, Kareem El-Badry, Yan-Fei Jiang, Semyeong Oh, and Hans-Walter Rix for useful discussions. The computations in this Letter were run on the Odyssey cluster supported by the FAS Division of Science, Research Computing Group at Harvard University. H.M.K. acknowledges support from the DOE CSGF under grant No. DE-FG02-97ER25308. C.C. acknowledges support from the Packard Foundation. Y.S.T. is supported by the NASA Hubble Fellowship grant *HST*-HF2-51425.001 awarded by the Space Telescope Science Institute. M.C.S. acknowledges financial support from the National Key Basic Research and Development Program of China (No. 2018YFA0404501) and NSFC grant 11673083.

This work has made use of data from the European Space Agency (ESA) mission Gaia (<https://www.cosmos.esa.int/gaia>), processed by the Gaia Data Processing and Analysis Consortium (DPAC, <https://www.cosmos.esa.int/web/gaia/dpac/consortium>). Funding for the DPAC has been provided by national institutions, in particular the institutions participating in the Gaia Multilateral Agreement.

This project was developed in part at the 2019 Santa Barbara Gaia Sprint, hosted by the Kavli Institute for Theoretical Physics at the University of California, Santa Barbara. This research was supported in part at KITP by the Heising-Simons Foundation and the National Science Foundation under grant No. NSF PHY-1748958.

ORCID iDs

Charlie Conroy  <https://orcid.org/0000-0002-1590-8551>

Yuan-Sen Ting  <https://orcid.org/0000-0001-5082-9536>

Ana Bonaca  <https://orcid.org/0000-0002-7846-9787>

References

- Alonso-Floriano, F., Caballero, J., Cortés-Contreras, M., Solano, E., & Montes, D. 2015, *A&A*, **583**, A85
- Andrews, J. J., Anguiano, B., Chanamé, J., et al. 2019, *ApJ*, **871**, 42
- Andrews, J. J., Chanamé, J., & Agüeros, M. A. 2017a, *MNRAS*, **473**, 5393
- Andrews, J. J., Chanamé, J., & Agüeros, M. A. 2017b, *MNRAS*, **472**, 675
- Bland-Hawthorn, J., & Gerhard, O. 2016, *ARA&A*, **54**, 529
- Bland-Hawthorn, J., Krumholz, M. R., & Freeman, K. 2010, *ApJ*, **713**, 166
- Bochanski, J. J., Faherty, J. K., Gagné, J., et al. 2018, *AJ*, **155**, 149
- Boubert, D., Strader, J., Aguado, D., et al. 2019, *MNRAS*, **486**, 2618
- Bovy, J. 2016, *ApJ*, **817**, 49
- Chanamé, J., & Gould, A. 2004, *ApJ*, **601**, 289
- Chen, B., Stoughton, C., Smith, J. A., et al. 2001, *ApJ*, **553**, 184
- Choi, J., Dotter, A., Conroy, C., et al. 2016, *ApJ*, **823**, 102
- De Silva, G. M., Freeman, K., Asplund, M., et al. 2007, *AJ*, **133**, 1161
- Deng, L.-C., Newberg, H. J., Liu, C., et al. 2012, *RAA*, **12**, 735
- Dotter, A., Conroy, C., Cargile, P., & Asplund, M. 2017, *ApJ*, **840**, 99
- El-Badry, K., & Rix, H.-W. 2018, *MNRAS*, **480**, 4884
- El-Badry, K., & Rix, H.-W. 2019, *MNRAS*, **482**, L139
- Gaia Collaboration, Brown, A. G. A., Vallenari, A., et al. 2018, *A&A*, **616**, A1
- Jiang, Y.-F., & Tremaine, S. 2010, *MNRAS*, **401**, 977
- Jiménez-Esteban, F. M., Solano, E., & Rodrigo, C. 2019, *AJ*, **157**, 78
- Kamdar, H., Conroy, C., Ting, Y.-S., et al. 2019, arXiv:1902.10719
- Kouwenhoven, M., Goodwin, S., Parker, R. J., et al. 2010, *MNRAS*, **404**, 1835
- Kroupa, P. 2001, *MNRAS*, **322**, 231
- Lindgren, L. 2018, Re-normalising the Astrometric Chi-square in Gaia DR2, Tech. Note GAIA-C3-TN-LU-LL-124, (Lund: Lund Observatory) http://www.rssd.esa.int/doc_fetch.php?id=3757412
- Lindgren, L., Hernández, J., Bombrun, A., et al. 2018, *A&A*, **616**, A2
- Luo, A.-L., Zhao, Y.-H., Zhao, G., et al. 2015, *RAA*, **15**, 1095
- Marchetti, T., Rossi, E. M., & Brown, A. G. A. 2019, *MNRAS*, **490**, 157
- Monroy-Rodríguez, M. A., & Allen, C. 2014, *ApJ*, **790**, 159
- Oelkers, R. J., Stassun, K. G., & Dhital, S. 2017, *AJ*, **153**, 259
- Oh, S., Price-Whelan, A. M., Brewer, J. M., et al. 2018, *ApJ*, **854**, 138
- Oh, S., Price-Whelan, A. M., Hogg, D. W., Morton, T. D., & Spergel, D. N. 2017, *AJ*, **153**, 257
- Parker, R. J., Goodwin, S. P., & Allison, R. J. 2011, *MNRAS*, **418**, 2565
- Poveda, A., Herrera, M., Allen, C., Cordero, G., & Lavalley, C. 1994, *RMxAA*, **28**, 43
- Price-Whelan, A. M., Oh, S., & Spergel, D. N. 2017, arXiv:1709.03532
- Recio-Blanco, A., de Laverny, P., Allende Prieto, C., et al. 2016, *A&A*, **585**, A93
- Reipurth, B., & Mikkola, S. 2012, *Natur*, **492**, 221
- Sartoretti, P., Katz, D., Cropper, M., et al. 2018, *A&A*, **616**, A6
- Shaya, E. J., & Olling, R. P. 2010, *ApJS*, **192**, 2
- Simpson, J. D., Martell, S. L., Da Costa, G., et al. 2018, *MNRAS*, **482**, 5302
- Ting, Y.-S., Rix, H.-W., Conroy, C., Ho, A. Y., & Lin, J. 2017, *ApJL*, **849**, L9
- Tokovinin, A., & Lépine, S. 2012, *AJ*, **144**, 102
- Weinberg, M. D., Shapiro, S. L., & Wasserman, I. 1987, *ApJ*, **312**, 367
- Wu, Y., Luo, A.-L., Li, H.-N., et al. 2011, *RAA*, **11**, 924
- Yoo, J., Chaname, J., & Gould, A. 2004, *ApJ*, **601**, 311